



The performance of $Zn_{1-x}Ce_xO$ nanoparticles thin films in sunlight exposure: synthesis, characterization and photocatalytic activity

Numan Salah^{a,*}, A. Hameed^{b,c}, M. Aslam^b, Saeed S. Babkair^d, F.S. Bahabri^e

^aCenter of Nanotechnology, King Abdulaziz University, Jeddah 21589, Saudi Arabia, Tel. +966 126951595; Fax: +966 126951566; email: nsalah@kau.edu.sa

^bCenter of Excellence in Environmental Studies (CEES), King Abdulaziz University, Jeddah 21589, Saudi Arabia, emails: hameedch@yahoo.com (A. Hameed), aslam312@gmail.com (M. Aslam)

^cNational Centre for Physics, Quaid-e-Azam University, Islamabad 44000, Pakistan

^dDepartment of Physics, King Abdulaziz University, Jeddah 21589, Saudi Arabia, email: s_babkair@hotmail.com

^eSciences Faculty for Girls, King Abdulaziz University, Jeddah 21589, Saudi Arabia, email: f_s_bahabri@hotmail.com

Received 25 November 2015; Accepted 5 February 2016

ABSTRACT

The $Zn_{1-x}Ce_xO$ nanoparticles thin films ($x = 0.01, 0.03, 0.05, 0.07,$ and 0.1) were deposited on glass substrates by pulsed laser deposition (PLD) technique with the view to use in photocatalytic water decontamination applications. The pre-synthesized Ce-doped ZnO targets of various Ce dopant levels were subjected to PLD for the deposition of films. The optical evaluation of the Ce-doped compared to pure ZnO thin films by diffuse reflectance spectroscopy (DRS), revealed the dependence of the extension of the absorption edge in the visible region with the increasing Ce contents, whereas the shifts in the Raman spectra verified the insertion of Ce in the lattice. The structural and morphological characterization of the fabricated films was carried out by XRD, FESEM, and AFM. The variations in the oxidation states of the components of the films during the deposition were evaluated by XPS. The photocatalytic activity of the Ce-doped films, in comparison to bare ZnO, was evaluated in natural sunlight exposure for the removal of 2-chlorophenol. The as-fabricated Ce-doped films exhibited substantially high degradation/mineralization activity as well as stability against the photocorrosion as compared to pure ZnO. The film with 3% Ce contents showed the highest activity. The salient feature of the study was the low exposed area as compared to the overall size of the reactor. The kinetics of the photocatalytic degradation/mineralization process and the stability of the films in the repeated cycles were also evaluated.

Keywords: Sunlight photocatalysis; Nanoparticles thin film; 2-chlorophenol; Ce^{3+} doped ZnO

1. Introduction

Although with the discovery of cheap and non-toxic semiconducting materials such as TiO_2 and ZnO, photocatalysis has been recognized as the leading

technique for environmental remediation, however, the requirement of UV light as excitation source because of the wide bandgaps has restricted its commercial scope [1–7]. The cost and associated limitations in the use of artificial UV light have restricted photocatalysis to academic research. The natural sunlight that carries 3–5% UV and 46% visible photon

*Corresponding author.

being ample, free, ever renewable can be a suitable alternative as an excitation source but requires the development of narrow bandgap active photocatalysts with the capability to engage a major portion of the solar spectrum [8,9]. Various techniques are reported in the literature to shrink the wide bandgap materials for better spectral response and activity. The alteration of the band structure by inserting the metal ions in the lattice without disturbing the crystal structure is a suitable tool in this contest. The inserted metal ions not only improve the spectral response by lowering the conduction band, but also improve the delivery of the excited electrons to the adsorbed species [10–14]. The alteration of the existing wide bandgap materials such as TiO_2 and ZnO by metal doping in powder form and casting thin films is a popular area of research [15–18]. The use of pure and doped photocatalysts in powder form is abundant however, the thin films are rarely used in photocatalytic applications. Although already existing, the abundant use of nanoparticles has further intensified the concern on the removal of photocatalysts after decontamination process. The use of thin films as immobilized photocatalysts can completely eliminate the issue of retrieval.

Although ZnO is comparable to TiO_2 , both in terms of chemical and photocatalytic properties, however, its extended absorption cross section augments its suitability for sunlight photocatalytic applications. The photocatalytic studies in the sunlight exposure using pure or modified ZnO films are rare. Some recent studies have been reported on the use of ZnO -based thin films for water treatment using UV light as excitation source [19–22]. Although, few studies regarding the fabrication of metal doped ZnO films by PLD are reported in the literature [23,24], however, the experimental protocol which we adopted is completely different from the reported procedures. Additionally, the studies regarding the use of Ce^{3+} doped films for the removal of 2-CP particularly in sunlight exposure are rare.

In this work, we fabricated 4×2.5 cm pure and Ce^{3+} doped zinc oxide (ZnO) nanoparticles thin film using pulse laser deposition technique by the targets of the pre-synthesized Ce^{3+} doped ZnO powders. The current work is motivated by our previous work [25,26], in which we reported the excellent photocatalytic activity of Ce^{3+} surface modified ZnO powder. The Ce^{3+} doping level was varied from 1 to 10 (atom)% to fabricate $\text{Zn}_{1-x}\text{Ce}_x\text{O}$ ($x = 0.01, 0.03, 0.05, 0.07, \text{ and } 0.1$) films. The as-produced films were characterized by different techniques like UV-vis, DRS, Raman spectroscopy, XRD, XPS, AFM, and FESEM.

The salient feature of the study was the estimation of the photocatalytic activity of the Ce^{3+} doped ZnO thin film by exposing the 10 cm^2 glass substrate film with the photocatalyst layer of ~ 90 nm in a glass reactor with the area of 189 cm^2 containing 100 cm^3 of 2-CP solution. The degradation was measured by HPLC, whereas the mineralization was assessed by total organic carbon (TOC) measurements. Several other parameters were also studied.

2. Experimental details

In the current study, $\text{Zn}_{1-x}\text{Ce}_x\text{O}$ ($x = 0.01, 0.03, 0.05, 0.07, \text{ and } 0.1$) nanoparticles were synthesized by sol-gel technique. Appropriate amount of $\text{Zn}(\text{NO}_3)_2 \cdot 6\text{H}_2\text{O}$ (Sigma-Aldrich, 99.99% pure) and $\text{Ce}(\text{NO}_3)_3 \cdot 6\text{H}_2\text{O}$ (Sigma-Aldrich, 99.99% pure) were used as the sources of Ce^{3+} and Zn^{2+} ions. To synthesize the $\text{Zn}_{0.99}\text{Ce}_{0.01}\text{O}$ having 1% atomic ratio of Ce/Zn , 4.50 g of zinc nitrate and 0.0309 g of cerium nitrate were dissolved in 2:1 ratio of deionized water and ethanol mixture under constant stirring for two hours at 80°C . The mixture of metal ion solution was slowly hydrolyzed with dropwise addition of 0.1 M KOH solution and adjusted the pH at 8. The obtained gel was heated at 200°C till the complete transformation of gel to precipitates. The precipitates were filtered, thoroughly washed with water and acetone/ethanol mixture (50:50) for the complete removal of unreacted KOH, and dried in hot air oven overnight. The dried powder was grinded and calcined at 500°C in a muffle furnace for six hours. Other compositions of $\text{Zn}_{1-x}\text{Ce}_x\text{O}$ photocatalyst containing different Ce/Zn ratio were also prepared accordingly.

Pulse laser deposition (PLD) technique was applied for the synthesis of $\text{Zn}_{1-x}\text{Ce}_x\text{O}$ ($x = 0.01, 0.03, 0.05, 0.07, \text{ and } 0.1$) films at different concentrations by using the PLD system, Neocera Pioneer 180, Neocera, USA. In a typical deposition, a 1-inch pallet of synthesized photocatalytic powder material was pressed as a target for PLD system hydraulic pressing. Krypton fluoride laser medium was used to generate Excimer Laser at 248 nm and the laser power was adjusted at 270 mJ. The deposition on a glass slide was done at room temperature located above the target by ~ 12 cm. The number of pulses was 12,000 and the pressure was adjusted to 10 mtorr by using the oxygen gas with a flow rate of 30 sccm. The films were annealed at 500°C for 1 h. For the structural and morphological characterization of synthesized thin films, a field emission scanning electron microscopy (FESEM JSM-7500F, JEOL) and tapping mode atomic force microscopy

(AFM, UHVAFM/STM model XA 50/500), Omicron, Germany with the scanning area of $0.5 \times 0.5 \mu\text{m}$ were used. UV–vis diffuse reflectance spectrophotometer (DRS) equipped with an integrating sphere recorded the solid-state absorption and diffuse reflectance spectra of the synthesized thin films in 200–900 nm range. The bandgap was evaluated by extrapolating the curve obtained by plotting $(F(R) \times hv)^{1/2}$ vs. hv , where, $F(R)$ is the Kubelka-Munk transformations of the %R values in diffuse reflectance spectra. Raman shifts were measured with a DXR Raman microscope (Thermo Scientific, USA) using a 13 mW power and 780 nm laser as the excitation source. The crystal structure and phase purity of the material assimilated from X-ray diffraction (XRD, Ultima-IV diffractometer Rigaku, Japan) with Cu $K\alpha$ radiation source. X-ray photoelectron spectroscopy (XPS) measurements were carried out using a PHI 5000 (VersaProbe, Japan). The samples were irradiated with monochromatic Al $K\alpha$ radiation ($hv = 1,486.6 \text{ eV}$). Survey scans were performed using a step size of 0.25 eV/step. The obtained curves were fitted using *Multipack v8.2c* data analysis software, which was provided with the PHI-5000 VersaProbe ESCA instrument, using a combination of Gaussian and Lorentzian peak shapes. The photocatalytic performance of the Ce^{3+} doped films, in comparison to pure ZnO, was evaluated for the degradation of 2-chlorophenol (2-CP). In a typical experiment, the film was submerged in 100 ml of 20 ppm 2-CP solution in a Pyrex[®] glass reactor. The dimensions of the reactor are mentioned in our previous communication [5,27]. The coated portion was directed towards the direction of sunlight. The experiments were performed in the natural environment without controlling any parameters such as temperature and pressure. To estimate the adsorption, the 2-CP submerged films were kept in the dark for 30 min prior to the exposure. The solution was exposed to sunlight with an illumination of $1,050 \pm 50 \times 10^2 \text{ lx}$ during fixed period of daylight for 240 min. To monitor the progress of degradation process, the samples were drawn at regular intervals and subjected to HPLC (HPLC, (SPD-20A, Shimadzu Corporation, Japan) analysis. The samples for TOC (TOC-VCPH total carbon analyzer, Shimadzu Corporation, Japan), IC (Thermo scientific, USA, ion chromatograph, Dionex (ICS-5000 + EG) Eluent Generator) and ICP-AES (Shimadzu, Japan) analysis were also collected at the same time. The experiments in the visible region of the sunlight were performed by using Pyrex[®] glass as UV cutoff filter. The stability of the Ce^{3+} doped ZnO was evaluated by using the same film and fresh 2-CP solution in the five successive cycles.

3. Results and discussion

3.1. “Films” characterizations

The absorption spectra of pure and $\text{Zn}_{1-x}\text{Ce}_x\text{O}$ ($x = 0.01, 0.03, 0.05, 0.07, \text{ and } 0.1$) films is presented in 300–800 nm range are compared in Fig. 1. The initial observation was the enhanced absorption in the visible region as well as unique single absorption edges. These observations lead to the conclusion that the fabrication procedure, PLD, inserted Ce in the lattice of the ZnO without the formation of individual surface oxides. Probably, the alteration of the conduction band of ZnO composed of Zn^{2+} ($3d^{10}4s^0$) by the implanted Ce ($4f^1$) bands consequences the enhanced absorption of the films in the visible region. The setting up of the additional levels below or beside the existing conduction bands generates additional transitions by sharing the common O 2p valence band. With the increase in the impurity level, the magnitude of the transitions involving the parallel conduction band established by the Ce entities is increased that, consequences the augmented absorption in the visible region. The evaluation of the bandgaps of the Ce-doped films by plotting $(F(R) \times hv)^{1/2}$ vs. photon energy (hv), where $F(R)$ is the Kubelka-Munk transformation of the reflectance data, also resulted in the red shifted bandgap energies compared to ZnO with the unique absorption edges that verified the skeletal insertion of Ce. This result is presented in the inset shown in Fig. 1. The evaluated bandgaps for pure and $\text{Zn}_{1-x}\text{Ce}_x\text{O}$ ($x = 0.01, 0.03, 0.05, 0.07, \text{ and } 0.1$) films were $\sim 3.15, \sim 3.05, \sim 2.97, \sim 2.95, \sim 2.9, \text{ and } \sim 2.88 \text{ eV}$.

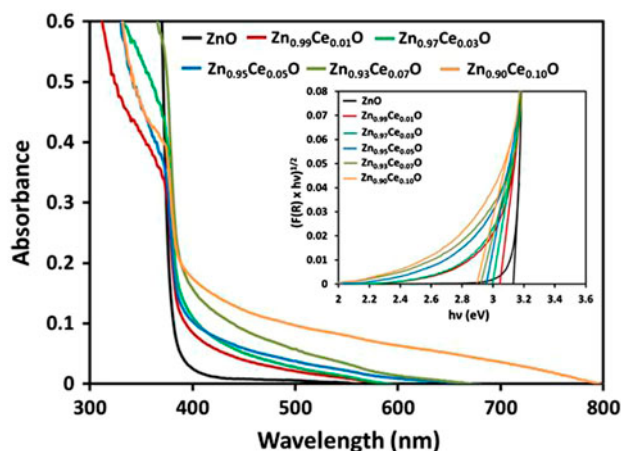


Fig. 1. Comparison of the solid state absorption spectra of pure and $\text{Zn}_{1-x}\text{Ce}_x\text{O}$ ($x = 0.01, 0.03, 0.05, 0.07, \text{ and } 0.1$) films in 300–800 nm. The inset shows the graphical evaluation of the bandgaps of the fabricated films.

The Raman spectra of the pure and Ce-doped ZnO films in 300–700 cm^{-1} range are presented in Fig. 2. In the current study, we exclusively concentrated on the E_2 (high) vibrational mode that corresponds to the Zn–O lattice stretching vibrations. In the pure ZnO film, the E_2 mode at $\sim 439 \text{ cm}^{-1}$ was in accordance with the literature values [28]. A noticeable shifting in the E_2 band, for the $\text{Zn}_{1-x}\text{Ce}_x\text{O}$ films, depicted the increased stiffness or more restricted stretching vibrations as compared to Zn–O bond that identified the insertion of Ce in the lattice thus leading to Zn–O–Ce type structures. Such type of observations are already reported for a similar type of systems [29]. The increasing level of Ce in the films substantially enhanced the activity of the band, however, its overall position remain preserved for all the Ce-doped films. Moreover, the appearance of additional bands probably representing the vibrations of Ce–O and Ce–O–Ce type structures.

In the XRD analysis, the major reflections for pure ZnO film at the 2θ values of 31.8° , 34.5° , 36.2° , 47.6° , 56.8° , 63.1° , and 68.0° corresponded to (1 0 0), (0 0 2), (1 0 1), (1 0 2), (1 1 0), (1 0 3), and (1 1 2) planes. These values were in close agreement with the literature values of highly crystalline hexagonal ZnO wurtzite structure [30]. The XRD patterns of the deposited polycrystalline $\text{Zn}_{1-x}\text{Ce}_x\text{O}$ films ($x = 0.01, 0.03, 0.05, 0.07, \text{ and } 0.1$) is presented in Fig. 3. In all the patterns, the careful analysis revealed no additional peak, corresponding to the supplementary phase that indicated the phase purity of the films. Concentrating on the (1 0 1) plane at 36.2° for pure ZnO, the reflection was shifted to 37.34° . The shift in the position of the reflec-

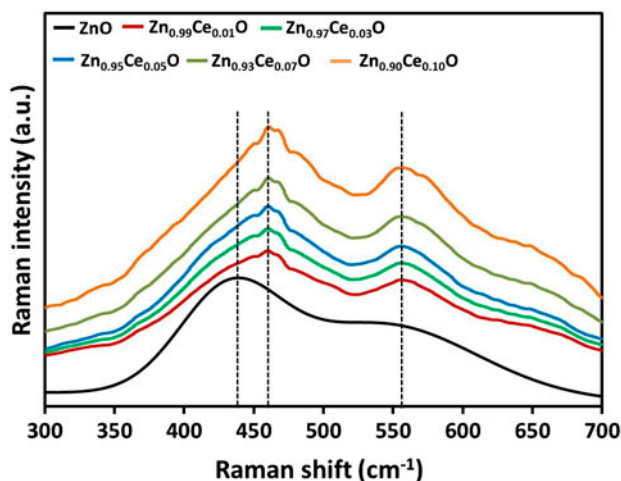


Fig. 2. Comparison of the Raman spectra of pure and $\text{Zn}_{1-x}\text{Ce}_x\text{O}$ ($x = 0.01, 0.03, 0.05, 0.07, \text{ and } 0.1$) films in the wavelength range of 300–700.

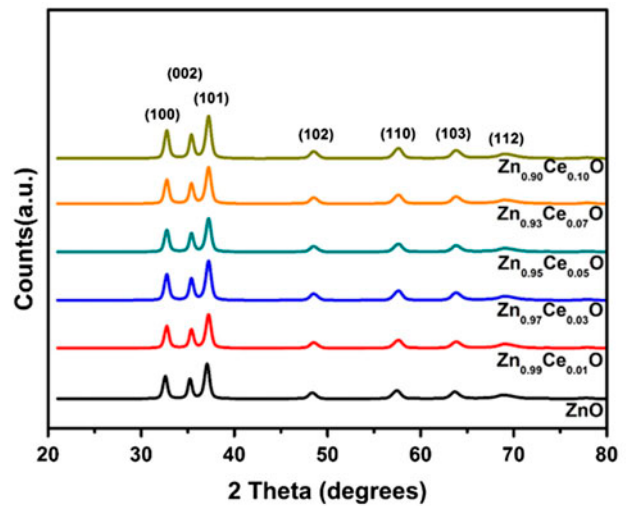


Fig. 3. Comparison of the solid state absorption spectra of $\text{Zn}_{1-x}\text{Ce}_x\text{O}$ ($x = 0.01, 0.03, 0.05, 0.07, \text{ and } 0.1$) films in the 2θ range of 20–80°.

tion was attributed to the strain introduced in the film with the insertion of Ce that causes a change in the diffraction angle [31].

The wide angle XPS survey scan of $\text{Zn}_{0.95}\text{Ce}_{0.05}\text{O}$ film is presented in Fig. 4(a) where the peaks at different binding energies represented the components (Ce, Zn, O) of the film. The deconvolution and fitting of the raw peak $\text{Ce}3d_{5/2}$ exposed at least four peaks at the binding energies of ~ 880.95 , ~ 883.84 , ~ 886.21 , and $\sim 888.12 \text{ eV}$ (Fig. 4(b)). As mentioned in the experimental details, Ce^{3+} was used as the precursor for the synthesis of the Ce-doped ZnO powder initially and fabrication of $\text{Zn}_{1-x}\text{Ce}_x\text{O}$ ($x = 0.01, 0.03, 0.05, 0.07, \text{ and } 0.1$) films finally, the appearance of the peaks corresponding to 3+ and 4+ oxidation states revealed the oxidation states transformation during the fabrication process. The intense peaks at ~ 883.84 and $\sim 886.21 \text{ eV}$ represented the Ce in 3+ oxidation state, whereas the low intensity peaks at 880.95 and 888.12 eV identified the 4+ oxidation states. The coexistence of 3+ and 4+ oxidation states of Ce is well documented in the literature [32–34]. The asymmetry was observed in the high resolution scans of $\text{Zn}2p$ and $\text{O}1s$ core levels due to the changed chemical environment in $\text{Zn}_{1-x}\text{Ce}_x\text{O}$ ($x = 0.01, 0.03, 0.05, 0.07, \text{ and } 0.1$) films compared to pure ZnO. As presented in Fig. 4(c), the deconvolution of the asymmetric peak of $\text{Zn}2p_{3/2}$ levels revealed the intense peak at 1,020.07 eV and low intensity peak at $\sim 1,021.62 \text{ eV}$. Although both of these peaks represented Zn in 2+ oxidation, however, indicated different chemical environments. The asymmetry in the shape of the peak indicated the initiation of the additional peaks of oxygen from the chemically differ-

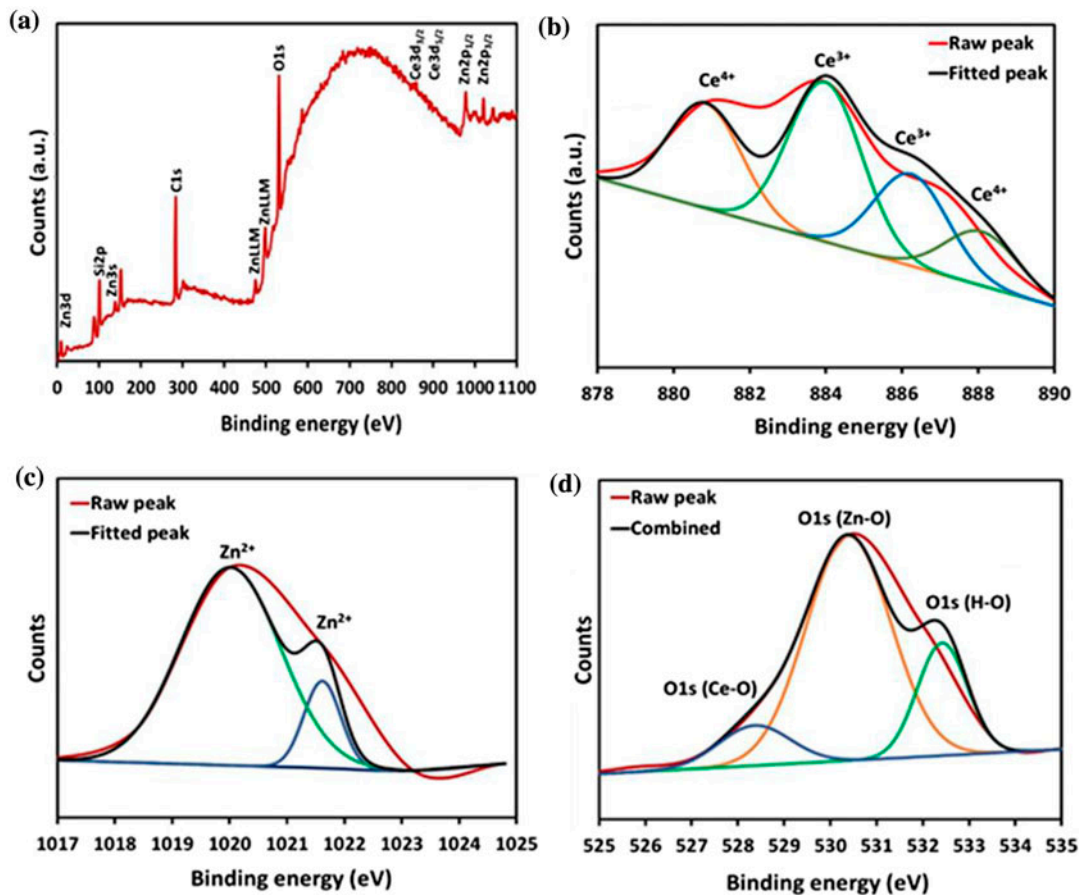


Fig. 4. (a) The wide angle survey scan of 5 atom% Ce doped ZnO film whereas (b)–(d) shows the deconvolution and curve fitting of the high precision scans of Ce3d_{5/2}, Zn2p and O1s core levels, respectively.

ent origin. The deconvolution of the asymmetric O1s narrow-angle scan is presented in Fig. 4(d). The intense peak at ~530.5 eV represented the majority oxygen attached to Zn in ZnO whereas the low intensity peaks at ~528.4 and ~532.44 eV were assigned to the oxygen attached to Ce(III, IV) and the surface hydroxyl groups, respectively.

The FESEM images of Zn_{0.95}Ce_{0.05}O film at the magnification of 15,000 \times and 120,000 \times are compared in Fig. 5(a) and (b), respectively. The images showed the even deposition of the particles without cracks or blank spaces. It is evident from the images that the nanostructures with a uniform morphology are formed with the adopted experimental conditions. The particle size distribution ranged between 20 and 30 nm. The particles appeared as the aggregates of the smaller particles that resulted in the random shapes. The morphology and particle size of the other films of different Ce concentrations are similar to those shown in Fig. 5(a) and (b). Such types of findings are disclosed earlier [35].

To confirm the particle size deposited on the glass slides by the PLD system, typical AFM images were recorded and presented in this study. Fig. 6(a) and (b) shows two-dimensional and three-dimensional AFM images of Zn_{0.95}Ce_{0.05}O film. The observed morphology is similar to that shown by SEM images. Nanoparticles with sizes around 20–25 nm can be seen. Some aggregated clusters are observed, but with a slight height, which cannot significantly affect the deposition quality. The other films of different Ce concentrations exhibited similar features in their structure and morphology. No significant changes in the particle size or shape are observed by increasing the dopants concentration. Perhaps the change in the particle size and shape is negligible and could not be observed at this ultrafine structure.

3.2. Photocatalytic studies

It is very well established that a cascade of ionic, radical and molecular species is generated in the

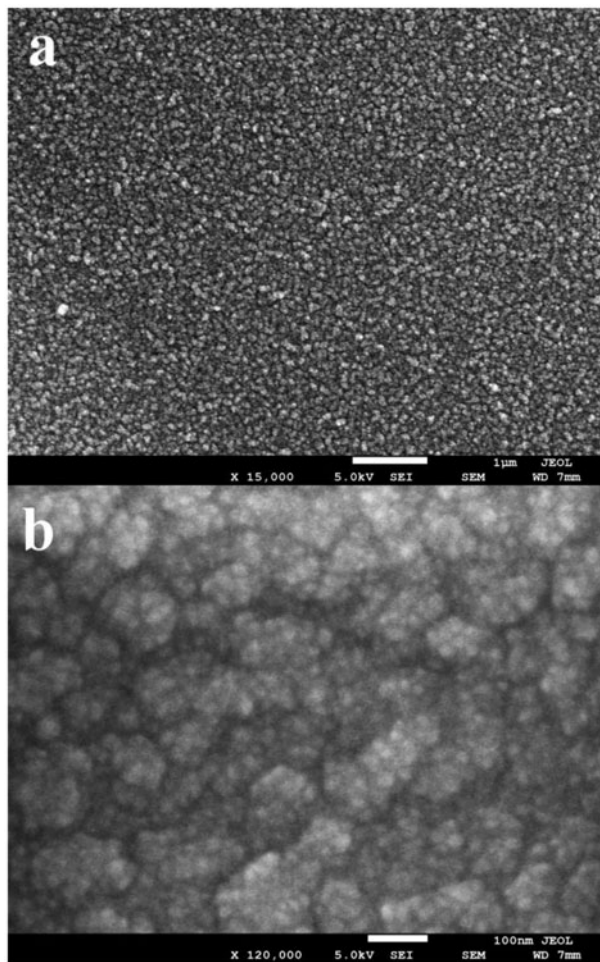


Fig. 5. The typical FESEM images of 5 atom% Ce doped ZnO film at (a) 15,000 \times and (b) 120,000 \times .

photocatalytic system with the interaction of photons having energy sufficient enough to excite the valence band electrons across the bandgap barrier. The oxygen bearing ionic and radical entities are classified as reactive oxygen species (ROS). The superoxide anion and hydroxyl radicals are the primary oxidants that are believed to be generated instantaneously by the absorption of photons. The generation and life span of the ROS are dependent on the suitability of the potential associated with the band edges in the aqueous medium and pH of the system. Although, the hydroxyl radicals are assigned as the major contributors in the oxidation of the substrates in almost all the communications in the area of photocatalysis however, based on the experimental facts, the stance of the scientific community is diverting towards the superoxide anion radicals as the leading oxidants as some recent studies have questioned not only the formation but also the involvement in the degradation mechanism

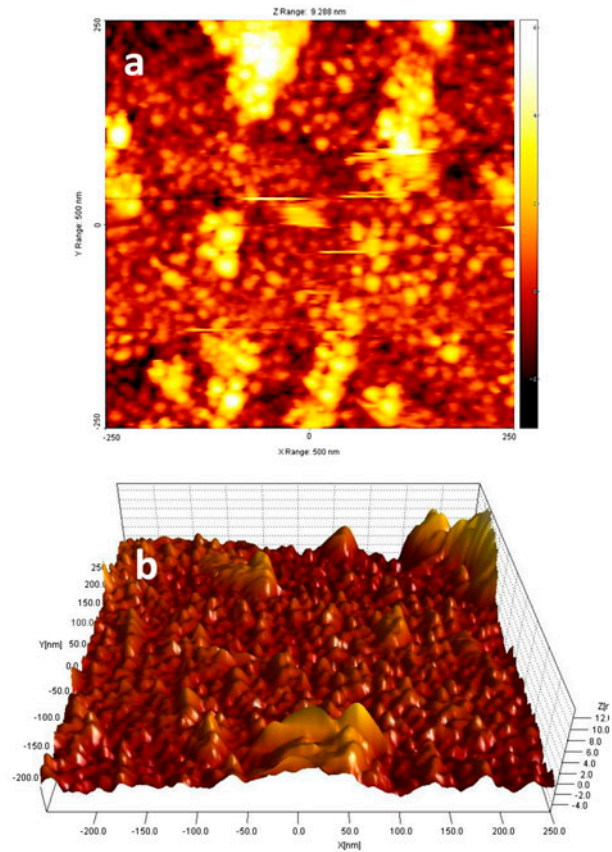


Fig. 6. The typical AFM images of 5 atom% Ce doped ZnO film (a) two dimensional and (b) three dimensional.

[36,37]. We believe that the careful analysis of the experimental data of the photocatalytic degradation studies can lead to the clues regarding the nature and role of the ROS involved in the degradation process.

The interesting feature of the current study is the assessment of the photocatalytic activity of the pure and Ce-doped ZnO films, having a significantly lower area available for exposure as compared to the total area of the reactor. Additionally, the films were immobilized in the middle of the reactor and no stirring or shaking was applied. The adsorption of the 2-CP substrate on pure and Ce³⁺ doped ZnO films was evaluated by comparing the peak heights of the samples collected after the dark experiments with that of 2-CP, 20 ppm standard. Compared to >20% for pure ZnO, The average adsorption of 2-CP on the Ce-doped films was <10%. A successive decrease in the adsorption was noticed with the increasing Ce³⁺ contents of the doped films.

As evaluated from the decrease in the HPLC peak heights, the percentage degradation of 2-CP for the pure ZnO and Zn_{1-x}Ce_xO films ($x = 0.01, 0.03, 0.05, 0.07, \text{ and } 0.1$) as a function of sunlight exposure time

is presented in Fig. 7(a). The comparison of the degradation curves for each film revealed the significantly higher activity of the Ce^{3+} doped films as compared to un-doped ZnO film. The activity of $\text{Zn}_{0.99}\text{Ce}_{0.01}\text{O}$, $\text{Zn}_{0.97}\text{Ce}_{0.03}\text{O}$, $\text{Zn}_{0.95}\text{Ce}_{0.05}\text{O}$, and $\text{Zn}_{0.93}\text{Ce}_{0.07}\text{O}$ films was comparable with each other, however, the activity of film doped with 3 atom% of Ce^{3+} was the highest among all. A decreasing trend was observed with the increase in the Ce^{3+} loading beyond 3 atom% Ce^{3+} doping and the minimum activity among all the doped films was noticed for 10 atom% Ce^{3+} doped ZnO film that was comparable with that of pure ZnO film. Compared to 20% removal for pure ZnO, the Ce-doped films degraded ~44, ~52, ~42, ~36 and ~24% of the 2-CP substrate in 30 min of sunlight exposure. The 1, 3, and 5 atom% Ce^{3+} doped ZnO films removed

≥90% of 2-CP in 120 min of exposure. All the films managed to remove >95% of the substrate in 240 min of exposure. The representative HPLC profile for the removal of 2-CP when $\text{Zn}_{0.97}\text{Ce}_{0.03}\text{O}$ film was exposed to sunlight is presented in Fig. 7(b), where the simultaneous removal of the substrate, as well as the intermediates, formed during the degradation process, is observable. The rate constants for the degradation of 2-CP in the presence of pure and Ce-doped films were calculated by plotting $\ln(C_0/C)$ vs. the exposure time as per Langmuir–Hinshelwood kinetic model for pseudo-first order reactions and presented in the inset of Fig. 7(a). A deviation from the kinetic model was observed for pure ZnO and $\text{Zn}_{0.90}\text{Ce}_{0.10}\text{O}$ film as a linear increase in the rate was noticed till ~70% removal of 2-CP substrate. A sharp increase deviating from linearity was observed afterward. The increased rate of degradation with the decreased concentration of 2-CP indicated the ample availability of the ROS for the degradation process as the overall number of ROS remains constant for a particular system. The observed rate constants for $\text{Zn}_{0.99}\text{Ce}_{0.01}\text{O}$, $\text{Zn}_{0.97}\text{Ce}_{0.03}\text{O}$, $\text{Zn}_{0.95}\text{Ce}_{0.05}\text{O}$, and $\text{Zn}_{0.93}\text{Ce}_{0.07}\text{O}$ films were 0.021, ~0.069, 0.020, and 0.018 min^{-1} , respectively.

The mineralization of 2-CP substrate during the degradation process for the pure, $\text{Zn}_{0.99}\text{Ce}_{0.01}\text{O}$, $\text{Zn}_{0.97}\text{Ce}_{0.03}\text{O}$, $\text{Zn}_{0.95}\text{Ce}_{0.05}\text{O}$, $\text{Zn}_{0.93}\text{Ce}_{0.07}\text{O}$, and $\text{Zn}_{0.9}\text{Ce}_{0.1}\text{O}$ films is presented in Fig. 8(a). Compared to pure ZnO film, a substantially high TOC removal was noticed for all the Ce^{3+} doped films except $\text{Zn}_{0.9}\text{Ce}_{0.1}\text{O}$ film. Keeping in view the organic content of 11.2 mg/L for 20 mg/L 2-CP, the $\text{Zn}_{0.97}\text{Ce}_{0.03}\text{O}$, and $\text{Zn}_{0.95}\text{Ce}_{0.05}\text{O}$ films reduced the TOC level below 1 mg/L that represents more than 90% TOC removal in 240 min of exposure. Consistent with our previous observations [25,26], the rate of TOC removal was significantly lower than the rate of the degradation process in the initial one hour that disclosed the priority of the ROS for the substrate. Additionally, the multistep nature of the mineralization process as compared the degradation was also exposed. The presence of the intermediates in the HPLC profile (Fig. 7(b)) also validates the same arguments. It can also be speculated that the larger intermediate fragments further interact to form smaller fragments which are mineralized accordingly. The rates of TOC removal are presented in Fig. 8(b). As expected, the rates of mineralization were significantly lower than those of degradation. The evaluated rates of mineralization for the pure ZnO film and $\text{Zn}_{1-x}\text{Ce}_x\text{O}$ films ($x = 0.01, 0.03, 0.05, 0.07,$ and 0.1) were 0.0052, 0.0074, 0.011, 0.0095, 0.0064, and 0.0046 min^{-1} , respectively. An increase in the rate of TOC removal was observed with the decreasing 2-CP concentration.

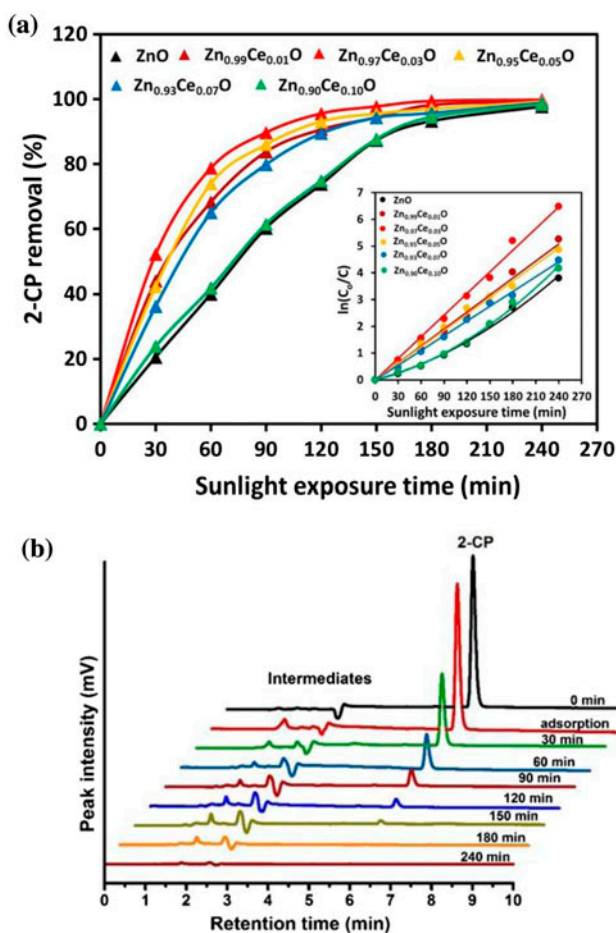


Fig. 7. (a) The percentage degradation of 2-CP for the pure ZnO and $\text{Zn}_{1-x}\text{Ce}_x\text{O}$ films ($x = 0.01, 0.03, 0.05, 0.07,$ and 0.1) as a function of sunlight exposure time and (b) the representative HPLC profile for the removal of 2-CP when $\text{Zn}_{0.97}\text{Ce}_{0.03}\text{O}$ film was exposed to sunlight. The inset of (a) shows the graphical evaluation of rate constants.

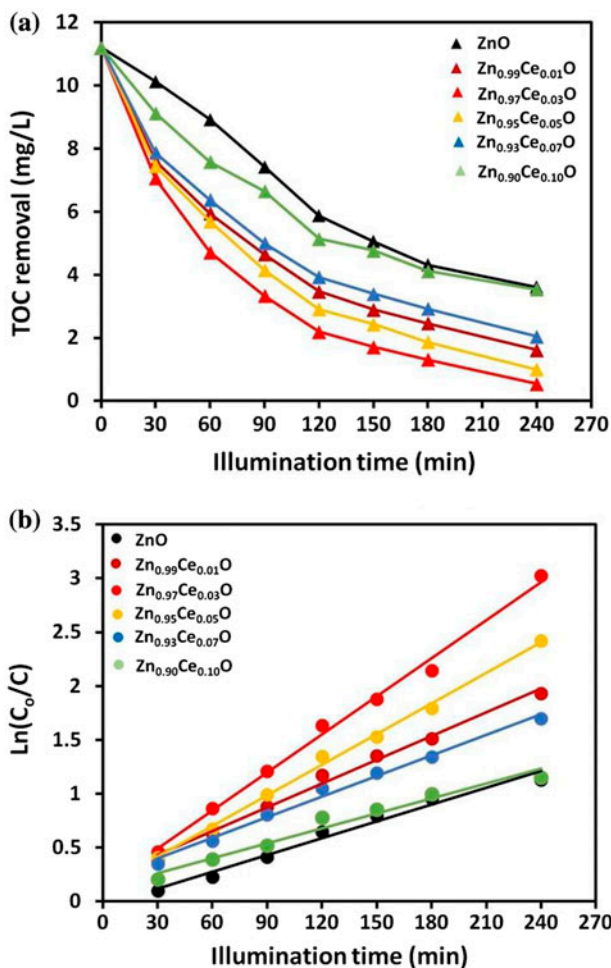


Fig. 8. (a) Comparison of TOC (mg/L) removal and (b) graphical evaluation of rate constants for mineralization during the degradation of 2-CP for the pure ZnO and Zn_{1-x}Ce_xO films ($x = 0.01, 0.03, 0.05, 0.07,$ and 0.1) as a function of sunlight exposure time.

Apart from ZnO film doped with 10 atom% of Ce³⁺, the activity of the other doped film was significantly higher than that of pure ZnO film that indicated the efficient role of the inserted Ce in suppressing the excitons recombination process by trapping the conduction band electrons and effective transfer of the trapped electrons for the enhanced generation of the ROS. It might be presumed that the excited electrons from the conduction band of Zn²⁺ (3d¹⁰4s¹) to the additional levels composed of Ce³⁺ (4f¹) orbitals of the impurity. Probably, the capture of the electron results in the increased energy that is dissipated instantaneously with the transfer of electrons. The highest activity of the film doped with 3 atom% Ce³⁺ indicates the optimum level of the doping. Beyond that limit, the electron transfer ability is reduced, that affects the overall generation of ROS in

the system. Regarding the identification of the major contributor among the primary ROS i.e. O₂⁻ and HO[•], the suitability of the conduction band potential of ZnO (-0.31 V) indicate the feasibility of higher generation of superoxide anions as compared to hydroxyl radicals. Additionally, the pH_{ZPC} (9.1) of ZnO also supports the extended lifetime of superoxide anions [37].

To estimate the mechanism and the nature of the ROS involved, the ions generated during the degradation process were monitored by ion chromatography (IC). The representative IC profile for the release of ions during the degradation process in the presence 3 atom% Ce-doped ZnO film is presented in Fig. 9(a). Interestingly, the concentration of the Cl⁻ ions was significantly lower than the expected value of 5.52 ppm for the completely dechlorinated 20 ppm 2-CP. An additional peak at the retention time of 8.2205 min whose identification with the standard revealed as ClO₂⁻ ion is also observable. The conversion to ClO₂⁻ ions was identified as the source of the low concentration of Cl⁻ ions in the solution. From

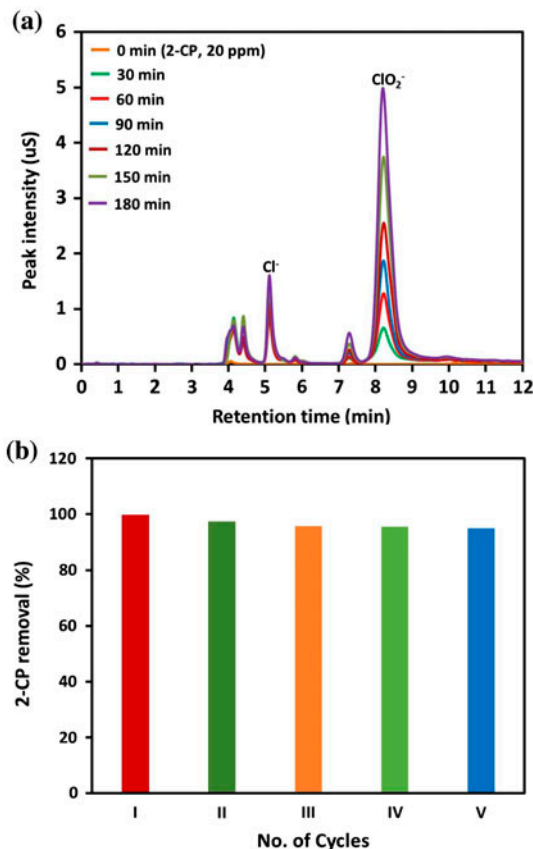


Fig. 9. (a) IC profile for the released ions and (b) the evaluation of film for reusability in five successive cycles for Zn_{0.97}Ce_{0.03}O film.

these observations, it can be anticipated that the Cl groups of the 2-CP are displaced by the negative charge bearing superoxide anions as the displacement of a charged group by the neutral hydroxyl radicals does not sound feasible that refers the major involvement of O_2^- rather than HO^\cdot . It can also be speculated that the interaction of O_2^- ions not only displace the Cl^- ions but also disintegrates the aromatic ring leading to the formation of smaller fragments that are interacted further to complete mineralization. The released Cl^- ions initially interact with photon generated holes (h^+) to form Cl^\cdot radicals. The interaction of O_2^- in the solution form ClO_2^- ions. The same is explained by the set of equations below:



The reusability plot of 3 atom% Ce-doped ZnO film is presented in Fig. 9(b). A mildly acceptable decrease in the activity of the film was observed after five successive cycles. The adsorption of the released inorganic may be the probable reason for this effect.

4. Conclusions

Ce doping not only enhanced the spectral response, but also the photocatalytic activity of ZnO. The charge trapping and transfer ability of the inserted Ce^{3+} augmented the generation of ROS in the system for efficient removal of 2-CP substrate. The study established the viability of the photocatalytic decontamination processes by exposing the active area of much smaller size as compared to the total area of the reactor. The lower rate of mineralization as compared to degradation disclosed the multistep nature of mineralization process that proceeds through the formation of intermediates. The escalated removal of 2-CP with the release of Cl^- and associated ions revealed the major contribution of superoxide anions in the photocatalytic process. The released Cl^- ions are converted to ClO_2^- ions by h^+ oxidation and superoxide interaction. The use of thin films and sunlight for the photocatalytic decontamination of water may eliminate the issues of high cost and photocatalysts removal.

Acknowledgements

This project was funded by the Scientific Waqf, King Abdulaziz University (KAU), Jeddah, Saudi Arabia under Grant No. 15/1435. The authors, therefore,

acknowledge with thanks to KAU Waqf for their technical and financial support. A. Hameed and M. Aslam are thankful to the Center of Excellence in Environmental Studies (CEES), King Abdulaziz University and Ministry of Higher Education (MoHE), Kingdom of Saudi Arabia, for their supports.

References

- [1] M. Aslam, I.M.I. Ismail, S. Chandrasekaran, H.A. Qari, A. Hameed, How the dyes are degraded/mineralized in a photocatalytic system? the possible role of auxochromes, *Water, Air, Soil Pollut.* 226(70) (2015) 1–15.
- [2] A. Fujishima, T.N. Rao, D.A. Tryk, Titanium dioxide photocatalysis, *J. Photochem. Photobiol., C* 1 (2000) 1–21.
- [3] D.F. Ollis, H. Al-Ekabi, *Photocatalytic Purification and Treatment of Water and Air*, Elsevier, Amsterdam, 1993, p. 207.
- [4] M.T. Qamar, M. Aslam, I.M.I. Ismail, N. Salah, A. Hameed, Synthesis, characterization, and sunlight mediated photocatalytic activity of CuO coated ZnO for the removal of nitrophenols, *ACS Appl. Mater. Interfaces* 7 (2015) 8757–8769.
- [5] M.H. Hernández-Alonso, F. Fresno, S. Suárez, J.M. Coronado, Development of alternative photocatalysts to TiO_2 : Challenges and opportunities, *Energy Environ. Sci.* 2 (2009) 1231–1257.
- [6] M. Aslam, M. Soomro, I.M.I. Ismail, H.A. Qari, M.A. Gondal, A. Hameed, The facile synthesis, characterization and evaluation of photocatalytic activity of bimetallic $FeBiO_3$ in natural sunlight exposure, *RSC Adv.* 5 (2015) 102663–102673.
- [7] J. Schneider, M. Matsuoka, M. Takeuchi, J. Zhang, Y. Horiuchi, M. Anpo, D.W. Bahnemann, Understanding TiO_2 photocatalysis: Mechanisms and materials, *Chem. Rev.* 114 (2014) 9919–9986.
- [8] A. Hameed, M. Aslam, I.M.I. Ismail, N. Salah, P. Fornasiero, Sunlight induced formation of surface $Bi_2O_{4-x}-Bi_2O_3$ nanocomposite during the photocatalytic mineralization of 2-chloro and 2-nitrophenol, *Appl. Catal. B: Environ.* 163 (2015) 444–451.
- [9] M.T. Qamar, M. Aslam, I.M.I. Ismail, N. Salah, A. Hameed, The assessment of the photocatalytic activity of magnetically retrievable ZnO coated $\gamma-Fe_2O_3$ in sunlight exposure, *Chem. Eng. J.* 283 (2016) 656–667.
- [10] X. Bai, L. Wang, R. Zong, Y. Lv, Y. Sun, Y. Zhu, Performance enhancement of ZnO photocatalyst via synergic effect of surface oxygen defect and graphene hybridization, *Langmuir* 29(9) (2013) 3097–3105.
- [11] U.I. Gaya, A.H. Abdullah, Heterogeneous photocatalytic degradation of organic contaminants over titanium dioxide: A review of fundamentals, progress and problems, *J. Photochem. Photobiol., C* 9 (2008) 1–12.
- [12] S.G. Kumar, L.G. Devi, Review on modified TiO_2 photocatalysis under UV/visible light: Selected results and related mechanisms on interfacial charge carrier transfer dynamics, *J. Phys. Chem. A* 115(46) (2011) 13211–13241.
- [13] S.G. Kumar, K.R.S. Koteswara Rao, Zinc oxide based photocatalysis: Tailoring surface-bulk structure and related interfacial charge carrier dynamics for better environmental applications, *RSC Adv.* 5 (2015) 3306–3351.

- [14] S. Rehman, R. Ullah, A.M. Butt, N.D. Gohar, Strategies of making TiO₂ and ZnO visible light active, *J. Hazard. Mater.* 170 (2009) 560–569.
- [15] R. Janisch, P. Gopal, N.A. Spaldin, Transition metal-doped TiO₂ and ZnO-present status of the field, *J. Phys.: Condens. Matter* 17 (2005) R657–89.
- [16] N.V. Kaneva, D.T. Dimitrov, C.D. Dushkin, Effect of nickel doping on the photocatalytic activity of ZnO thin films under UV and visible light, *Appl. Surf. Sci.* 257 (2011) 8113–8120.
- [17] J.L. Yang, S.J. An, W.I. Park, G.C. Yi, W. Choi, Photocatalysis using ZnO thin films and nanoneedles grown by metal-organic chemical vapor deposition, *Adv. Mater.* 16 (2004) 1661–1664.
- [18] A. Zaleska, Doped-TiO₂: A Review, *Recent Pat. Eng.* 2 (2008) 157–164.
- [19] V. Etacheri, R. Roshan, V. Kumar, Mg-doped ZnO nanoparticles for efficient sunlight-driven photocatalysis, *ACS Appl. Mater. Interfaces* 4(5) (2012) 2717–2725.
- [20] H. Qin, W. Li, Y. Xia, T. He, Photocatalytic activity of heterostructures based on ZnO and N-doped ZnO, *ACS Appl. Mater. Interfaces* 3(8) (2011) 3152–3156.
- [21] A. Sáenz-Trevizo, P. Amézaga-Madrid, P. Pizá-Ruiz, O. Solís-Canto, C. Ornelas-Gutiérrez, S. Pérez-García, M. Miki-Yoshida, Microstructural characterization, optical and photocatalytic properties of bilayered CuO and ZnO based thin films, *J. Alloys Compd.* 615 (2014) S375–S381.
- [22] S. Xiao, L. Zhao, X. Leng, X. Lang, J. Lian, Synthesis of amorphous TiO₂ modified ZnO nanorod film with enhanced photocatalytic properties, *Appl. Surf. Sci.* 299 (2014) 97–104.
- [23] E. Manikandan, V. Murugan, G. Kavitha, P. Babu, M. Maaza, Nanoflower rod wire-like structures of dual metal (Al and Cr) doped ZnO thin films: Structural, optical and electronic properties, *Mater. Lett.* 131 (2014) 225–228.
- [24] S. Thanka Rajan, B. Subramanian, A.K. Nanda Kumar, M. Jayachandran, M.S. Ramachandra Rao, Fabrication of nanowires of Al-doped ZnO using nanoparticle assisted pulsed laser deposition (NAPLD) for device applications, *J. Alloys Compd.* 584 (2014) 611–616.
- [25] M. Aslam, I.M.I. Ismail, S. Chandrasekaran, T. Almeelbi, A. Hameed, The suitability of Ce³⁺-modified ZnO photocatalyst for the mineralization of monochlorophenol isomers in sunlight exposure, *RSC Adv.* 4 (2014) 49347–49359.
- [26] I.M.I. Ismail, M. Aslam, T. Almeelbi, S. Chandrasekaran, A. Hameed, Ce³⁺ impregnated ZnO: A highly efficient photocatalyst for sunlight mediated mineralization, *RSC Adv.* 4 (2014) 16043–16046.
- [27] M. Aslam, M.T. Qamar, M.T. Soomro, I.M.I. Ismail, N. Salah, T. Almeelbi, M.A. Gondal, A. Hameed, The effect of sunlight induced surface defects on the photocatalytic activity of nanosized CeO₂ for the degradation of phenol and its derivatives, *Appl. Catal. B: Environ.* 180 (2016) 391–402.
- [28] D.E. Zhang, J.Y. Gong, J.J. Ma, G.Q. Han, Z.W. Tong, A facile method for synthesis of N-doped ZnO mesoporous nanospheres and enhanced photocatalytic activity, *Dalton Trans.* 42 (2013) 16556–16561.
- [29] M.F. Cerqueira, A.G. Rolo, T. Viseu, J. Ayres de Campos, T. de Lacerda-Arôso, F. Oliveira, M.I. Vasilevskiy, E. Alves, Raman study of doped-ZnO thin films grown by rf sputtering, *ys. Status Solidi C* 7 (2010) 2290–2293.
- [30] A. Iqbal, A. Mahmood, T.M. Khan, E. Ahmed, Structural and optical properties of Cr doped ZnO crystalline thin films deposited by reactive electron beam evaporation technique, *Prog. Nat. Sci.: Mater. Int.* 23 (2013) 64–69.
- [31] S.M. Salaken, E. Farzana, J. Podder, Effect of Fe-doping on the structural and optical properties of ZnO thin films prepared by spray pyrolysis, *J. Semicond.* 34(7) (2013) 1–6.
- [32] E. Paparazzo, XPS studies of damage induced by X-ray irradiation on CeO₂ surfaces, *Surf. Sci.* 234 (1990) L253–L258.
- [33] H.Y. Zhu, T. Hirata, Ce3d and Zr3d X-ray photoelectron spectroscopy spectra of ZrO₂-12 mol% CeO₂ after heat-treatments and Ar⁺ etching, *J. Mater. Sci. Lett.* 12 (1993) 749–751.
- [34] M. Aslam, M. Qamar, M. Soomro, I.M.I. Ismail, Z.A. Rehan, M. Ashraf, A. Hameed, The effect of cerium alteration on the photocatalytic performance of WO₃ in sunlight exposure for water decontamination, *RSC Adv.* 6 (2016) 2436–2449.
- [35] D. Wu, M. Long, W. Cai, C. Chen, Y. Wu, Low temperature hydrothermal synthesis of N-doped TiO₂ photocatalyst with high visible-light activity, *J. Alloys Compd.* 502 (2010) 289–294.
- [36] M.A. Henderson, A surface science perspective on TiO₂ photocatalysis, *Surf. Sci. Rep.* 66 (2011) 185–297.
- [37] P. Pichat, *Photocatalysis and Water Purification*, first ed., Wiley-VCH Verlag, Weinheim, 2013.